AMERICAN SOCIETY FOR MICROBIOLOGY | Applied and Environmental Microbiology®

ENVIRONMENTAL MICROBIOLOGY

Dynamics of Solitary Predation by *Myxococcus xanthus* on *Escherichia coli* Observed at the Single-Cell Level

Wenchao Zhang,[a] Yan Wang,[b] Huining Lu,[a] Qin Liu,[a] Chuandong Wang,[b] Wei Hu,[b] Kun Zhao[a]

[a]Frontier Science Center for Synthetic Biology and Key Laboratory of Systems Bioengineering (MOE), School of Chemical Engineering and Technology, Tianjin University, Tianjin, China

[b]State Key Laboratory of Microbial Technology, Microbial Technology Institute, Shandong University, Qingdao, China

ABSTRACT The predatory behavior of *Myxococcus xanthus* has attracted extensive attention due to its unique social traits and inherent biological activities. In addition to group hunting, individual *M. xanthus* cells are able to kill and lyse prey cells; however, there is little understanding of the dynamics of solitary predation. In this study, by employing a bacterial tracking technique, we investigated *M. xanthus* predatory dynamics on *Escherichia coli* at the single-cell level. The killing and lysis of *E. coli* by a single *M. xanthus* cell was monitored in real time by microscopic observation, and the plasmolysis of prey cells was identified at a relatively early stage of solitary predation. After quantitative characterization of their solitary predatory behavior, *M. xanthus* cells were found to respond more dramatically to direct contact with live *E. coli* cells than heat-killed or UV-killed cells, showing slower predator motion and faster lysing of prey. Among the three contact-dependent killing modes classified according to the major subareas of *M. xanthus* cells in contact with prey, leading pole contact was observed most. After killing the prey, approximately 72% of *M. xanthus* cells were found to leave without thorough degradation of the lysed prey, and this postresidence behavior is described as a lysis-leave pattern, indicating that solitary predation has low efficiency in terms of prey-cell consumption. Our results provide a detailed description of the single-cell level dynamics of *M. xanthus* solitary predation from both prey and predator perspectives.

IMPORTANCE Bacterial predation plays multiple essential roles in bacterial selection and mortality within microbial ecosystems. In addition to its ecological and evolutionary importance, many potential applications of bacterial predation have been proposed. The myxobacterium *Myxococcus xanthus* is a well-known predatory member of the soil microbial community. Its predation is commonly considered a collective behavior comparable to a wolf pack attack; however, individual *M. xanthus* cells are also able to competently lead to the lysis of a prey cell. Using a bacterial tracking technique, we are able to observe and analyze solitary predation by *M. xanthus* on *Escherichia coli* at the single-cell level and reveal the dynamics of both predator and prey during the process. The present study will not only provide a comprehensive understanding of *M. xanthus* solitary predation but also help to explain why *M. xanthus* often displays multicellular characteristic predatory behaviors in nature, while a single cell is capable of predation.

KEYWORDS predation, single-cell behavior, *Myxococcus xanthus*, *Escherichia coli*, tracking technique

Predator-prey interactions play significant roles in shaping the composition and regulating the dynamics of microbial ecosystems (1, 2). Many bacterial species have been observed to conduct predatory behaviors, e.g., *Lysobacter* spp. (3), *Herpetosiphon* spp. (4), *Bdellovibrio bacteriovorus* (5), and *Myxococcus xanthus* (6), while employing

Citation Zhang W, Wang Y, Lu H, Liu Q, Wang C, Hu W, Zhao K. 2020. Dynamics of solitary predation by *Myxococcus xanthus* on *Escherichia coli* observed at the single-cell level. Appl Environ Microbiol 86:e02286-19. https://doi.org/10.1128/AEM.02286-19.

Editor Hideaki Nojiri, University of Tokyo

Address correspondence to Wei Hu, hw_1@sdu.edu.cn, or Kun Zhao, kunzhao@tju.edu.cn.

Received 6 October 2019
Accepted 7 November 2019
Accepted manuscript posted online 8 November 2019
Published 21 January 2020

various strategies, i.e., epibiotic predation, endobiotic predation, direct invasion, and group attack (7). The first description of bacterial predation was the observation that some myxobacterial strains lysed other bacteria (7, 8), and to date, *M. xanthus* is the best-studied predatory myxobacterium due to its genetic tractability. *M. xanthus* has a sophisticated life cycle that involves vegetative swarming, predation when prey cells are present, and the formation of developmental multicellular biofilms (fruiting bodies) with myxospores embedded when nutrients are limited (6, 7, 9). As a social behavior, *M. xanthus* predation is described as a group hunting process using the myxobacterium-like strategy classified in the group attack category of bacterial predation (7). During the predation, *M. xanthus* cells use surface motilities to search for prey and produce a wide range of predatory products to kill and decompose the prey cells (10, 11).

M. xanthus cells hunt prey cells using a strategy comparable to a wolf pack attack (7, 12, 13), in which surface motility plays an important role (14, 15). *M. xanthus* possesses two independent surface motility systems, social motility (S motility) that is dependent on type IV pili (TFP) and exopolysaccharide (EPS) and adventurous motility (A motility) that drives isolated cells' gliding movement along their long axis in the absence of extracellular appendages (15–17). It has been shown that A and S motilities are both required for efficient *M. xanthus* predation (18–20). Moreover, by regulating the reversal frequency through a chemotaxis signaling Frz system, a group of *M. xanthus* cells is able to swarm toward nutrients (chemotaxis-like behavior) (19) or to prey colonies (predataxis behavior) (20).

Motion ability provides *M. xanthus* cells the advantage of actively searching for prey. To kill and to digest prey cells, *M. xanthus* produces a variety of degradative enzymes and specialized secondary metabolites with antibiotic properties, including myxovirescin (also known as antibiotic TA), myxalamid, and cittilin (21–24). Among them, TA has been suggested to be a major *M. xanthus*-diffusible antibacterial agent against live *Escherichia coli* cells (21, 25), while it showed no apparent effect in killing *Micrococcus luteus* (21), indicating that these active compounds might be selective for prey species. In addition, some subcellular structures such as outer membrane vesicles (OMVs) also play a critical role in *M. xanthus* predation, which might be responsible for delivering a complex mixture of metabolites and enzymes to the prey (24, 26).

While *M. xanthus* predation is commonly considered a collective behavior (13, 27, 28), individual *M. xanthus* cells are also able to competently lead to the lysis of a prey cell (29). McBride and Zusman (29) studied the predation on microcolonies of *E. coli* by single *M. xanthus* cells. They found that single wild-type *M. xanthus* cells were able to lyse and digest a whole *E. coli* microcolony, while *frz* mutant cells only digested part of prey cells in a microcolony, which indicates that *M. xanthus* is capable of performing solitary predation. However, the dynamics of *M. xanthus* solitary predation at the single-cell level are still not clear. Moreover, in group attack mode, only a few *M. xanthus* cells at the leading position of the hunting group have the opportunity to make contact with the prey directly, and most of the cells that do not reach the prey cells might be regulated by subsequent *M. xanthus* cell-cell interactions to direct their predatory behaviors. In that case, characterizing the solitary behavior will also help to understand the complex collective process of *M. xanthus* predation, which highlights the importance of solitary predation research. Until now, there have been relatively few quantitative studies on solitary predation, and our understanding of its mechanism is still very limited.

The aim of the present study was to observe and characterize *M. xanthus* solitary predation at the single-cell level, particularly, the dynamics of the process from both the prey and predator perspectives. By employing a bacterial tracking technique that enables long-time monitoring of cell behavior at the single-cell level, we report real-time observations of the dynamics of solitary predation by *M. xanthus* on *E. coli*.

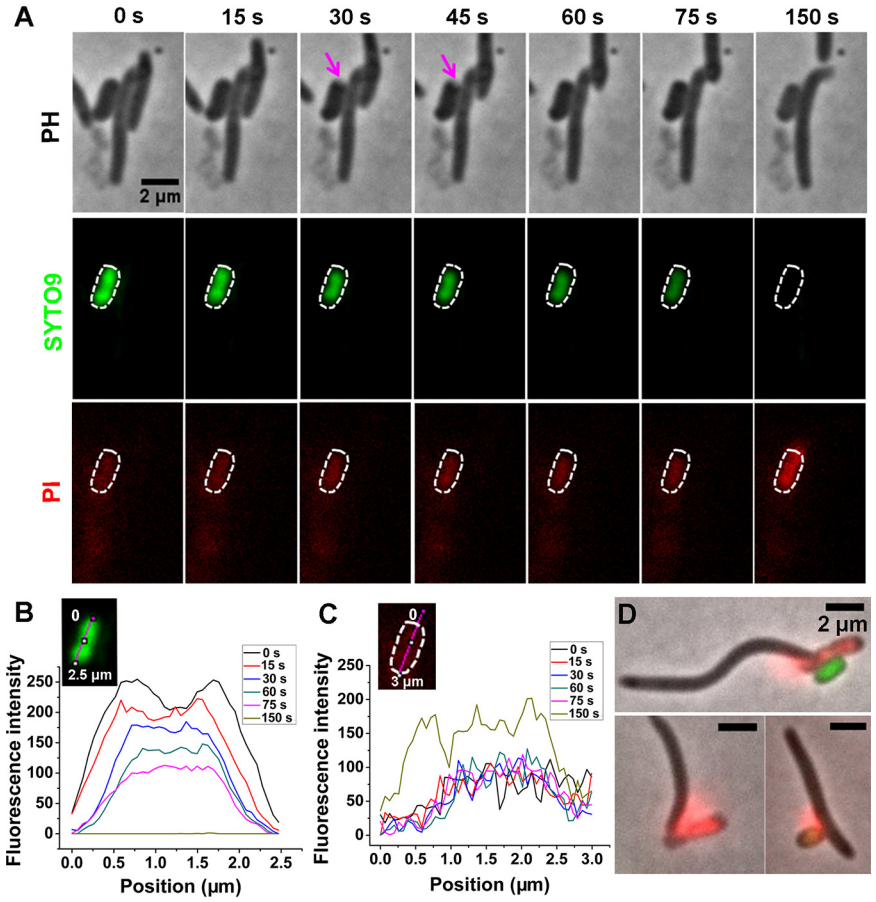

FIG 1 Observation of *E. coli* prey cells during predation. (A) Representative image sequence showing the changes of *E. coli* cells (short rod-like) caused by *M. xanthus* (long rod-like) predation observed in PH images and live/dead stained fluorescence images. The arrows indicate a relatively transparent bay area that appeared at one pole of an *E. coli* cell. The SYTO 9 panels show viable cells with intact cytoplasmic membranes (green), and the PI panels show dead cells with compromised membranes (red). For better observation, the corresponding scrutinized cell in the fluorescence images is outlined by dashed lines according to the PH images. The shooting time of the image is noted above the PH panels. (B and C) The green (B) and red (C) fluorescence intensities of the *E. coli* cells along the cell body axis (see solid line in the inset) at different time points during predation. (D) Merged images of PH and live/dead stained fluorescence images taken from another three experimental sets at the late stage of cell-cell contact between *M. xanthus* cells (long rod-like) and *E. coli* (short rod-like), showing the leaked DNA substances from the ruptured *E. coli* cells.

RESULTS AND DISCUSSION

Observation of physiological state and plasmolysis of *E. coli* during solitary predation by *M. xanthus*. To better understand the *M. xanthus* solitary predation process on *E. coli* cells, we first examined the morphology of *E. coli* cells (i.e., prey) during predation. As shown in Fig. 1A, *M. xanthus* (long rod-like) and *E. coli* (short rod-like) are relatively distinguishable by their cell morphology, and the physiological state of an *E. coli* cell is visualized by live/dead fluorescence staining. As predation continued, the fluorescence of the *E. coli* cell changed from a bright green color (SYTO 9 labeled, indicating live state) to a red color (propidium iodide [PI] labeled, indicating dead state), which is presumably due to the cytoplasmic membrane damage caused by the *M. xanthus* cell (see also Fig. S1 in the supplemental material). It should be noted that under our experimental conditions using a staining buffer with relatively low concentrations of SYTO 9 and PI, *M. xanthus* cells were not labeled by the fluorescent dyes (see Fig. S2). Figure 1B and C show quantitative measurements of the intensities of green and red fluorescence, respectively, along the body axis of the scrutinized *E. coli* cell shown in Fig. 1A. The green intensity gradually diminished and reached the

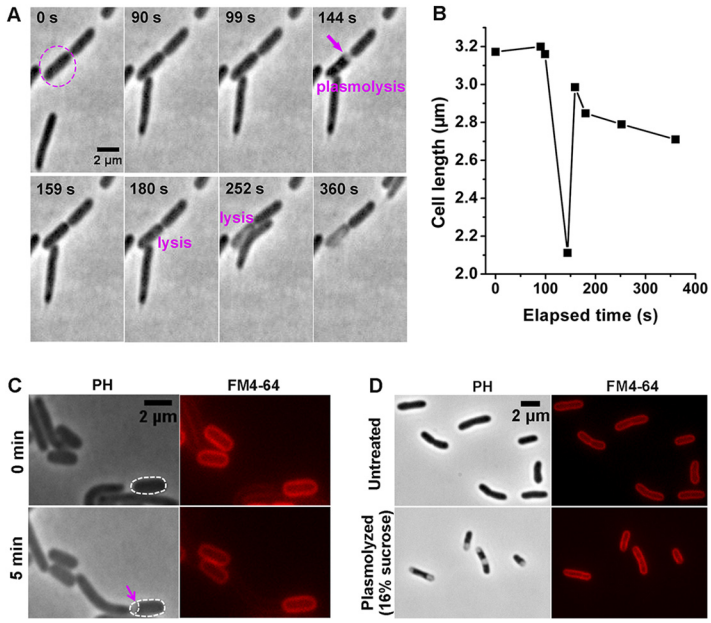

FIG 2 Plasmolysis event of *E. coli* during predation. (A) Representative image sequence showing *E. coli* plasmolysis caused by *M. xanthus* predation. (B) Cell length of *E. coli* in panel A measured over time. (C) FM4-64-stained images showing the intact outer membrane of an *E. coli* cell when a plasmolysis bay area formed during predation. (D) PH and membrane stained images of untreated *E. coli* cells (top) and plasmolyzed *E. coli* cells induced by a buffer containing a high concentration of sucrose (bottom).

background level at 150 s, whereas the red intensity increased over time and spread out of the cell envelope, indicated by a phase-contrast (PH) image, implying potential cell leakage at 150 s. The leaked DNA stained by PI is more obvious in the observations shown in Fig. 1D, which confirms that *E. coli* cells are lysed after contacting a single *M. xanthus* cell and suggests successful predatory events.

Interestingly, shrinkage of the *E. coli* prey cell can be observed in Fig. 1A. A relatively transparent bay area was apparent at one pole of the *E. coli* cell in the images taken at 30 to 45 s of the predation (indicated by arrows), and this observation was further confirmed by the additional experimental sets shown in Fig. 2 and Fig. S3, suggesting that plasmolysis of the *E. coli* cell occurred. The cell length of the selected *E. coli* cell shown in Fig. 2A (indicated by dotted circle) was measured (Fig. 2B), defined as the length of the dark region along the cell body axis in the PH images. The results showed that the cell length first decreased from ~3.2 μm at 0 s to a minimum (~2.1 μm) at 144 s and subsequently recovered to near the original length at approximately 159 s; cell lysis was clearly observed at 180 s. More measurements are shown in Fig. S3. To further confirm the observed plasmolysis, the outer membrane (OM) of the *E. coli* cell was visualized using dye FM4-64 (30, 31), and the results (Fig. 2C) show that while the length of the cell dark region in PH images retracts, the cell envelope (OM) is still complete without any noticeable change in size. The plasmolysis we observed during predation is similar to the plasmolysis of *E. coli* cells caused by hyperosmotic shock (Fig. 2D). When an *E. coli* cell is lysed, its OM is broken and the FM4-64-stained pattern is changed from an intact cell outline to a deflated-like OM (see Fig. S4).

Under our experimental conditions, approximately 52% of the observed predation events ($n = 105$) showed clear plasmolysis of *E. coli* cells. For those in which plasmolysis events were not observed, it is possible that plasmolysis happened so quickly that it was beyond the capability of our system to capture due to the limited time resolution, or some *E. coli* cells may have been directly lysed without showing plasmolysis. Since the plasmolysis of *E. coli* cells caused by contact with a single *M. xanthus* cell is similar to that observed with antibiotic treatment (32, 33) or hyperosmotic shock (31), it is possible that the vast amount of secondary metabolites produced by *M. xanthus* (21, 23) provide harsh conditions for *E. coli* prey cells at the early stage of predation.

Compared to that with live *E. coli* cells, when heat-killed *E. coli* cells were used as prey, no obvious cell length and morphological changes were observed (see Fig. S5A and B). Similarly, UV-killed *E. coli* cells, which may have intact cell membranes, also showed no obvious plasmolysis, and the morphology of dead *E. coli* cells remained unchanged at the early stage of predation (Fig. S5C). These results indicate that *M. xanthus* cells might respond differently to live and dead prey cells.

Behavior of *M. xanthus* solitary predation on live *E. coli* differs from that on heat- or UV-killed *E. coli*. To further investigate how *M. xanthus* responds to prey cells, we quantitatively characterized the motility of *M. xanthus* cells during their solitary predation on different *E. coli* cells on Tris-phosphate-magnesium (TPM) agar. Considering that physical contact between predator and prey is necessary for *M. xanthus* predation (34), the process of *M. xanthus* solitary predation was divided into two continuous stages: the no-contact-with-prey (NCWP) stage (that includes the seeking period) and the contact-with-prey (CWP) stage (that typically incorporates the killing and assimilate periods). The motility of *M. xanthus* cells at these two stages was investigated accordingly.

At the NCWP stage, for all cases using different *E. coli* cells as prey, the average instantaneous speeds of *M. xanthus* cells (red data in Fig. 3C, E, and G) obtained via Gaussian curve fitting were 2.5 $\pm$ 1.0 (mean $\pm$ standard deviation [SD]), 2.6 $\pm$ 1.1, and 2.5 $\pm$ 0.9 μm/min, respectively, which are all similar to the average speed of 2.3 $\pm$ 1.1 μm/min obtained when there is no prey cell present (Fig. 3A). However, at the CWP stage, the speed was 0.9 $\pm$ 0.7 μm/min for the case of live prey (black data in Fig. 3C), 1.7 $\pm$ 1.0 μm/min for heat-killed prey, and 1.8 $\pm$ 0.9 μm/min for UV-killed prey (black data in Fig. 3E and G). When contacting live *E. coli* cells, brief pauses of the *M. xanthus* cells were constantly marked by our tracking program, which is consistent with the previous observation that *M. xanthus* cells cease their movement for several minutes when they contact a microcolony of live *E. coli* prey (29). In contrast, *M. xanthus* cells were observed to slip over dead *E. coli* cells without any obvious pauses. The difference in motion behavior of *M. xanthus* cells could contribute to the observed speed differences in Fig. 3C, E, and G. Consistently, the distributions of deviation angles exhibit a similar trend (Fig. 3D, F, and H). At the NCWP stage, cells show a similar narrow distribution of deviation angle with a peak value close to 0 rad in all cases (i.e., the moving direction is along the cell body axis [red lines]). However, at the CWP stage, the distribution for live *E. coli* is wider than that for either heat-killed or UV-killed *E. coli*.

To quantitatively characterize *M. xanthus* single-cell motion during predation, mean square displacements (MSDs), which measure to what extent the motion deviates from a random walk, were also calculated (Fig. 3I). The results show that for all the tests, *M. xanthus* cells display superdiffusive motion, with MSD slopes of >1 (in log-log plot of MSDs). At the CWP stage, *M. xanthus* cells move slower when live *E. coli* cells are used than when either heat-killed or UV-killed *E. coli* cells are used as prey. These results again show that *M. xanthus* responds more actively to live *E. coli* cells than dead ones, which is also macroscopically confirmed using the swarming assay (see supplementary text and Fig. S6). To see whether the response of *M. xanthus* to live *E. coli* cells depends on the physiological states of prey, both live *E. coli* cells collected in the decline phase (see Fig. S7) and nondividing *E. coli* cells (data not shown) were also tested. In both cases, similar to that observed when using mid-log-phase prey cells, *M. xanthus* cells showed a pause when they contacted these prey cells. In addition, we also analyzed the predation of live *E. coli* by a small group of *M. xanthus* cells and found that the leading cell in the group showed an obvious pause with an instantaneous speed close to 0 when it contacted prey, whereas the following cells at the tail of the group passed through the same area directly with normal speed, possibly because the *E. coli* cells were already killed or lysed by the leading cell (see Fig. S8 and Movie S1).

The above-described results regarding motility characterization indicate that *M. xanthus* cells tend to slow down more remarkably when contacting live *E. coli* than dead *E. coli*. The longer contact with live prey might provide the predator more time to

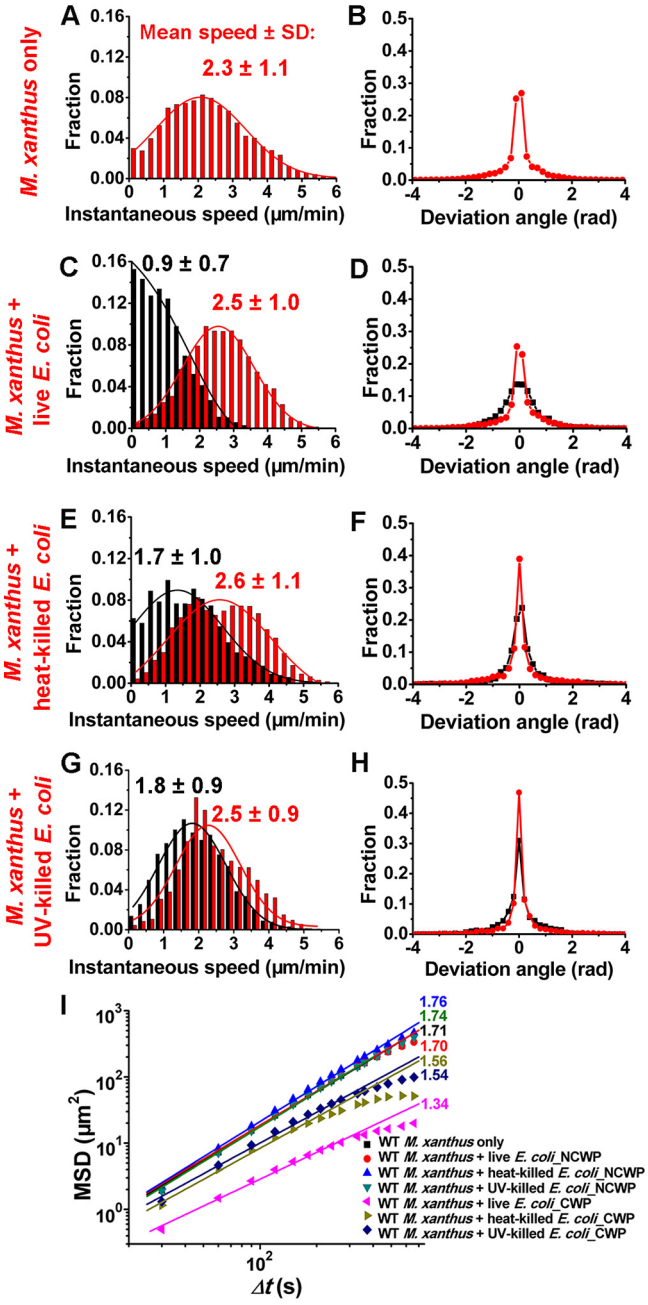

FIG 3 Motility characterization of *M. xanthus* cells in solitary predation. Distribution of instantaneous speed (A) and deviation angle (B) of *M. xanthus* cells without the addition of *E. coli* prey cells as a control. Distributions of instantaneous speeds of *M. xanthus* during predation on live (C), heat-killed (E), and UV-killed (G) *E. coli* cells. Lines are fitted Gaussian curves. The obtained mean values ± standard deviations (SDs) of instantaneous speeds (μm/min) are listed. Distributions of the deviation angles of *M. xanthus* during predation on live (D), heat-killed (F), and UV-killed (H) *E. coli* cells. In panels C to H, red data points represent the results when *M. xanthus* cells do not contact *E. coli* cells (NCWP stage), and black data points represent the results when *M. xanthus* cells directly contact *E. coli* cells (CWP stage). (I) MSDs of *M. xanthus* cells obtained under the seven circumstances. The solid lines are regression lines of each MSD data point in the log-log plot. The numbers of *M. xanthus* cells analyzed were 190, 100, 80, and 60 for the cases of no *E. coli*, live *E. coli*, heat-killed *E. coli*, and UV-killed *E. coli*, respectively.

prepare substances such as antibiotic metabolites or hydrolytic enzymes to kill and lyse its nearby prey, which, in principle, should lead to faster lysis for live prey cells versus dead ones. To test this hypothesis, red fluorescent protein (RFP)-expressing *E. coli* MG1655 cells were used as prey (Fig. 4). As expected, the RFP signal in live *E. coli* cells

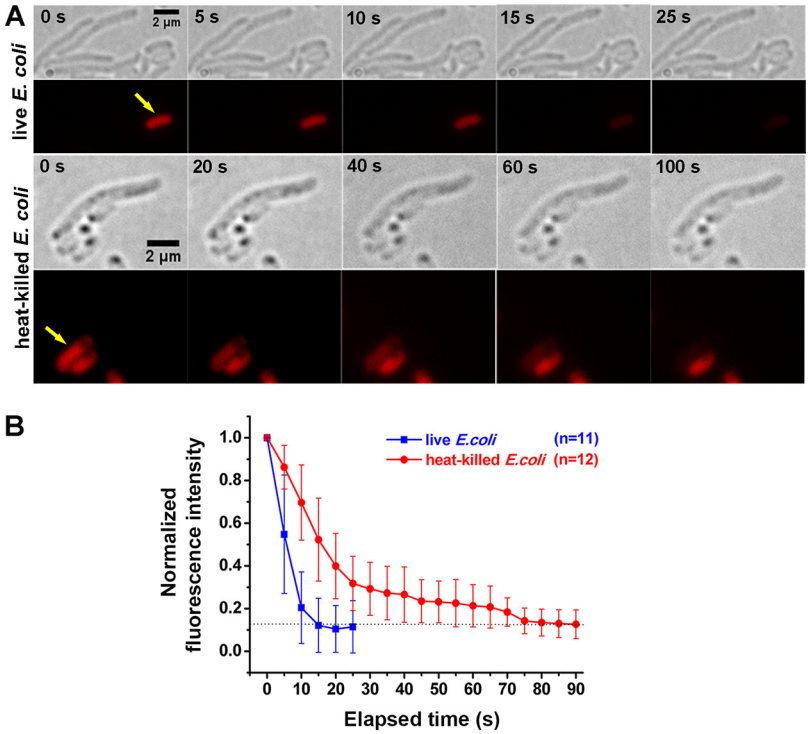

FIG 4 Differences between live and heat-killed RFP-expressing *E. coli* in the dynamics of predation-induced cell lysis. (A) Bright-field and fluorescence image sequences of *M. xanthus* preying upon live (top two rows) and heat-killed (bottom two rows) RFP-expressing *E. coli*. Yellow arrows indicate cells of interest. (B) Normalized fluorescence intensities of RFP-expressing *E. coli* cells during predation. The numbers of analyzed cells were 11 for live *E. coli* and 12 for heat-killed *E. coli* cells. Error bars represent standard deviations of the means.

decreased to the background level within a much shorter period of time (~20 s) than that in heat-killed *E. coli* (~90 s).

While our results support the hypothesis that *M. xanthus* is able to sense live from dead *E. coli* prey, the underlying mechanism remains elusive. Using liquid culture, Livingstone et al. (35) showed that the transcriptional response of *M. xanthus* to live *E. coli* prey was minimal, with only 12 genes significantly upregulated, whereas the response to dead *E. coli* cells was relatively more active, with altered expression of approximately 1,319 genes. This suggests that the predation response of *M. xanthus* to *E. coli* can be remarkably different under different culture conditions or experimental setups. Our attempts to reveal the transcriptional response of *M. xanthus* solitary predation on different *E. coli* cells were not successful due to the difficulty in collecting sufficient amounts of *M. xanthus* cells at the CWP stage.

Leading pole contact mode is observed most among the three killing modes employed by *M. xanthus*. Physical contact between predator and prey has been shown to be essential for *M. xanthus* predation (29, 34). The residence time is defined as the time of the short pause period when an *M. xanthus* cell contacts and stays still with a prey cell. For wild-type (WT) *M. xanthus* DK1622, the average residence time is 281 ± 127 s. While it has been shown that both A and S motilities are required for efficient *M. xanthus* predation (18–20), the residence time in our experimental setup was 270 ± 128 s for Δ*pilA* (A^+S^-) cells and 283 ± 170 s for Δ*aglZ* (A^-S^+) cells, suggesting that A and S motilities have less effect on the time for prey lysis. This could be explained by the fact that the residence time we measured started after predator and prey had been in physical contact, and the killing process (roughly during the residence time) would be much less affected by the predator's motility once it already detected the prey.

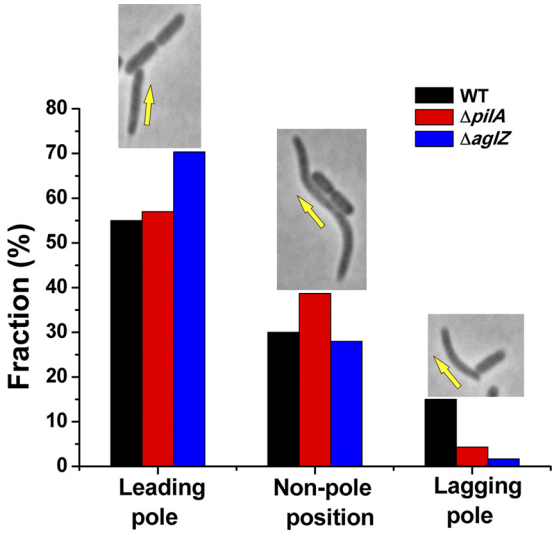

FIG 5 Distributions of contact modes during predation on live *E. coli* by WT, Δ*pilA*, and Δ*aglZ M. xanthus* cells. The numbers of analyzed predation events were 97 for WT, 93 for Δ*pilA*, and 118 for Δ*aglZ* cells. The yellow arrows in the insets indicate the moving direction of *M. xanthus* cells.

Considering the nonhomogeneous distribution of several types of apparatus on the cell surface of *M. xanthus*, such as type IV pili (TFP) (36, 37), a statistical analysis was performed to reveal the contact modes between *M. xanthus* and live *E. coli* cells during predation. While an *M. xanthus* cell contacts prey cells using its whole cell body, the contact modes can still be roughly classified into three categories based on the major contact subareas on an *M. xanthus* cell: leading pole contact, nonpole contact, and lagging pole contact, which are shown in Fig. 5 and Movies S2 to S4. For WT *M. xanthus*, approximately 55% of cells tend to use their leading pole to prey, while 30% use the nonpole part of the body and 15% of cells use the lagging pole for contact; thus, among the three modes, leading pole contact is observed most often. The average lengths of WT *M. xanthus* cells were measured to be 7.5 ± 1.6, 8.2 ± 1.9, and 7.4 ± 1.3 μm (mean $\pm$ SD) for cells of leading pole contact, nonpole position contact, and lagging pole contact, respectively. These results indicate that there is no obvious correlation between the cell length and the predation contact modes.

For Δ*pilA* cells, similar to WT, 57% of cells used the leading pole to prey, whereas for Δ*aglZ* cells, the percentage of such cells was 70%. Interestingly, the probability of using the lagging pole to prey was 4.3% for Δ*pilA* cells and 1.7% for Δ*aglZ* cells, which are both less than that for WT (15%). Such differences appear to correlate with the differences in the motility pattern of those mutants, where Δ*pilA* and Δ*aglZ* cells show more confined moving patterns than WT (see Fig. S9).

Solitary predation by *M. xanthus* is not efficient in terms of prey-cell consumption. The predation process includes not only searching and killing but also the consumption of prey. After the residence time, during which *M. xanthus* cells stay in contact to kill *E. coli* cells, will they continue to stay and consume the dead prey cells? The postresidence predator behavior was analyzed, and two types of moving pattern were observed. One was lysis-leave (LL), in which predator cells continued to move and left contact with prey cells via either moving out of the observation window or deviating from their original path and not contacting prey cells anymore (Movie S5). The other was lysis-stay (LS), in which predator cells moved around while keeping contact with prey cells by frequently reversing (Movie S6). For the LL cells, predator cells started to move away directly after the residence time and left the deflated-like prey cell residues behind. In contrast, for the LS cells, predator cells started to move again after the residence time and normally reversed before they left contact with prey cells; sometimes they were observed to reverse back even after they were clearly separated

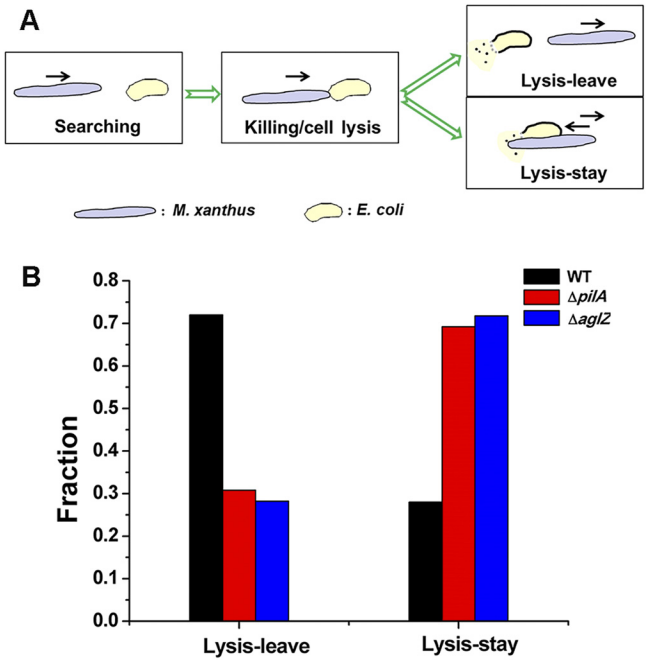

FIG 6 Postresidence moving patterns of *M. xanthus* cells in solitary predation. (A) A schematic model for *M. xanthus* solitary predation. (B) Measured fractions of two moving patterns (LL and LS) for WT ($n = 100$), Δ*pilA* ($n = 78$), and Δ*aglZ* ($n = 78$) cells.

from prey cells by a relatively short distance. Compared with that for LL, such prolonged contact with prey cells in the LS moving pattern presumably enables predators to consume more of the leaked cytoplasmic substances as well as cell envelopes, which results in much more distorted morphologies of prey cells. These observations suggest that *M. xanthus* cells showing LS might be able to consume the lysed prey cells for a longer time and profit more from their own killing behavior than those showing LL. A summarized schematic model for *M. xanthus* solitary predation is shown in Fig. 6A.

To quantitatively characterize the LL and LS patterns, we analyzed 100 events of WT *M. xanthus* cells after killing (Fig. 6B). Approximately 72% of WT cells showed the LL moving pattern, while only ~28% of WT cells showed the LS moving pattern. By continuously recording the surface evolution in the same field of view after *E. coli* cells were killed and lysed by LL cells, we further tracked the remaining *E. coli* cell fragments for a longer time (up to 12 h). We found that after a couple of passages by other *M. xanthus* cells, the *E. coli* cell fragments were gradually reduced (see Fig. S10), presumably due to the consumption by those passing *M. xanthus* cells. These results imply that for solitary predation in the majority of cases, WT *M. xanthus* cells kill prey cells while leaving a large part of the dead prey cells unconsumed, so solitary predation is not efficient in terms of prey-cell consumption. A possible explanation for this behavior is that a single *M. xanthus* cell is not able to produce sufficient amounts of degradative enzymes to completely consume the dead prey cells, since both cell density-dependent efficient predation (13) and cell density-dependent growth on the medium supplied with large molecular nutrients (12) have been suggested in *M. xanthus*. However, it is also possible that nutrient/stimulant signals produced by a single prey cell may not be sufficient to prevent *M. xanthus* from migrating away from lysed prey. In addition, approximately 28% of WT *M. xanthus* cells still exhibited the LS pattern of consuming most of their dead prey by reversing back and forth along the dead cells. Among those LS cells, the fraction of cells that reversed when they were just out of contact with prey (see examples in Fig. S11) was approximately 47%. This illustrates the important role of cell reversal to achieve efficient solitary predation, which is consistent with the previous observation that *frz* mutants lacking the ability to reverse were only able to lyse some

TABLE 1 Bacterial strains used in this study

Bacterial strain	Genotype or description	Reference or source
Myxococcus xanthus		
DK1622	Wild-type strain	41
DK10410	Δ*pilA*	42
MXH2265	Δ*aglZ*	43
Escherichia coli		
MG1655	Wild-type strain, K-12 substrain MG1655	ATCC
MG1655-1#	MG1655 harboring pRFP (RFP expressing)	This study

prey cells that they directly contacted while leaving prey microcolonies with substantially intact prey cells behind (29). Meanwhile, it has been proposed that the contact with prey cells is tracked by multiple Frz signaling clusters that are distributed along the entire *M. xanthus* cell body (13). When an *M. xanthus* cell moves outside the prey cells in proximity, the loss of prey signal detection might trigger a reversal and lead to a change in the direction of cell movement. Our findings fit well with this proposed model.

Similar analysis was also conducted on Δ*pilA* and Δ*aglZ* mutants (Fig. 6B). Interestingly, compared with that for the WT, these two motility mutants showed a higher fraction of LS cells (~70% for Δ*pilA* and ~72% for Δ*aglZ* cells). After following their cell trajectories, it was found that both mutants showed less of an exploratory pattern, which did not appear to be dependent on the presence of prey cells. This indicates that the observed higher fraction of LS likely derived from a partial motility deficiency rather than from a better response to prey cells (38).

Conclusions. In this work, we presented a real-time observation of solitary predation by *M. xanthus* on *E. coli*, and the dynamics of the process were characterized at the single-cell level using a bacterial tracking technique from both the prey and predator perspectives. The killing of *E. coli* by a single *M. xanthus* cell was confirmed with the observation of cytoplasmic membrane damage and DNA leakage of prey cells, and the real-time dynamics of plasmolysis in *E. coli* cells were also identified at a relatively early stage of solitary predation. Combined with single-cell behavior data for *M. xanthus* during predation, we found that the predator responded more dramatically to the presence of live prey than to the presence of dead prey, which supports that predation is a tug-of-war process incorporating responses from both predators and preys. A statistical analysis of contact-dependent killing modes showed that among these three modes, the leading pole contact mode is most likely to be observed during predation. Quantitative characterization of the moving pattern of predators after killing prey cells showed that approximately 72% of *M. xanthus* cells left without thoroughly degrading the lysed cells, indicating that solitary predation by *M. xanthus* is not efficient in terms of prey consumption. When performing group hunting, which is typically engaged by *M. xanthus* in natural environments, the problem of the low efficiency of solitary predation could be overcome by employing collective behaviors that facilitate fast cellular movement (39) and high cell density to guarantee a local concentration of active metabolites and degraded enzymes when encountering prey. In the future, by performing further tracking and quantification of the group predation behavior of *M. xanthus*, the mechanism of predation efficiency improvement by group action compared to that of solitary action will be revealed. This might shed light on understanding why *M. xanthus* often displays multicellular characteristic predatory behaviors in nature when single cells are also capable of predation.

MATERIALS AND METHODS

Bacterial strains and growth conditions. Bacterial strains used in this study are listed in Table 1. *E. coli* strains were used as prey and were cultured on Luria-Bertani (LB) medium containing 1.5% agar or in liquid LB broth at 37°C. The *M. xanthus* strains were grown to mid-log phase in Casitone-yeast extract (CYE) [1% (wt/wt) Casitone, 0.5% (wt/wt) yeast extract, 10 mM 3-(*N*-morpholino)propanesulfonic acid

(MOPS), 4 mM $MgSO_4 \cdot 7H_2O$, pH 7.6] liquid medium at 30°C on a rotary shaker at 200 rpm or on CYE plates containing 1.5% agar with the same components.

Predation assays. To initiate all predation assays, mid-log-phase *M. xanthus* cells (18 to 24 h in CYE broth) were harvested by centrifugation and washed twice with TPM buffer (10 mM Tris-HCl [pH 7.6], 8 mM $MgSO_4$, and 1 mM KH_2PO_4-K_2HPO_4 [pH 7.6]), and concentrated to a final optical density at 600 nm (OD_{600}) of ~0.6. A 2-μl droplet of cell suspension was added to the center of a 35-mm glass-bottom petri dish (NEST, Shanghai, China). Next, 2 μl of *E. coli* culture (OD_{600} of ~0.8, either live or heat-killed cells) was spotted and mixed with *M. xanthus* suspension. A 1.5% TPM agar pad was placed on top of the bacterial cells. Samples were mounted on the stage of an optical microscope, and appropriate observational fields of view were selected; then, samples were imaged as described below without moving the stage position during data collection. Images were captured every 3 s for ~18 h. Heat-killed *E. coli* cells were obtained by placing the cellular suspension in a forced-air drying oven for 10 min at 90°C.

UV-killed *E. coli*, *E. coli* in the decline phase, and nondividing *E. coli* cells were also used as prey in control experiments. To obtain UV-killed *E. coli* cells, 20-μl aliquots of the cellular suspension were dropped onto 1.5% TPM agar and exposed to UV light for 3 h (60 W). Then, 2 μl of *M. xanthus* suspension was spotted on the center of the glass bottom of a petri dish. A TPM agar pad containing UV-killed *E. coli* cells was placed on top of the *M. xanthus* cells for subsequent observations. *E. coli* cells in the decline phase were obtained by harvesting the cells after ~72 h of growth in LB liquid medium. Nondividing *E. coli* cells were prepared by treating mid-log-phase *E. coli* cells with 15 μg/ml cephalexin for 4 h.

Plasmolysis induced by hyperosmotic stress. To prepare the plasmolysis of *E. coli* induced by hyperosmotic stress, 1 ml of mid-log-phase *E. coli* cells (OD_{600} of ~0.8 to 1.6) from LB liquid culture was harvested and resuspended in 1 ml of plasmolysis solution (16% sucrose). Then, the plasmolyzed cells were visualized under a microscope within 15 min.

Fluorescence/time-lapse microscopy. Predation assays were monitored by a Leica DMi8 inverted microscope (Leica, Germany) equipped with an adaptive focus control system. Images were taken using an electron-multiplying charge-coupled-device (EMCCD) camera (Andor iXon Ultra 888). Bright-field images were acquired at 3-s intervals for a total of approximately 18 h, and the image size was 66.5 μm by 66.5 μm (1,024 × 1,024 pixels). Red fluorescence of RFP-expressing *E. coli* was detected with the rhodamine (Rhod) filter with an exposure time of 200 ms at 5-s intervals. The fluorescence intensity of RFP-expressing *E. coli* was corrected for background and normalized for comparison as follows: for each cell, corrected total cell fluorescence (CTCF) was first calculated as the integrated fluorescence intensity inside the cell area minus the cell area multiplied by the mean fluorescence of background readings. Then, the fluorescence intensity at time t was normalized by dividing the intensity value at t by the fluorescence intensity at $t = 0$ s. Fluorescence analysis was performed using ImageJ software.

Live/dead staining. For viability analysis of *E. coli* during predation, cell suspensions were stained with a mixture of SYTO 9 (5 μM final concentration) and PI (30 μM final concentration) provided in the LIVE/DEAD BacLight Bacterial Viability kit (L-7012; Molecular Probes, Eugene, OR, USA). Samples were incubated in the dark at room temperature for 15 min before analysis. Then, 2 μl of dye-labeled *E. coli* culture (OD_{600} of ~0.8) was spotted on the glass bottom of a petri dish and mixed with *M. xanthus* suspension. The bacterial cells were then covered with a 1.5% TPM agar pad. Fluorescence was measured using the fluorescein isothiocyanate (FITC) filter (live cells) and the Rhod filter (dead cells). Images were taken at 15-s intervals.

Plasma membrane labeling. Membranes were visualized by staining with the lipophilic dye FM4-64 (10 μg/ml final concentration; Molecular Probes, Eugene, OR, USA). *E. coli* cultures were incubated on ice for 2 min in the dark. Then, the predation assay was performed immediately as described above. Fluorescence was detected using the Rhod filter. Images were taken at 15-s intervals. *E. coli* labeled with FM4-64 and *M. xanthus* cells were added to a glass-bottom petri dish and covered with 1.5% TPM agar, and time-lapse phase-contrast microscopy was used to track cell movement. The image acquisition process was finished in a short time (no more than 0.5 h) to minimize FM4-64 uptake.

Bacterial tracking and singe-cell data analysis. Bright-field images (30-s intervals) were preprocessed using a combination of software and algorithms adapted from the methods described (39) and written in MATLAB R2015a (Mathworks) by subtracting the background, scaling, smoothing, and thresholding to convert to binary images via Otsu thresholding. The bacterial shape was fit to a spherocylinder, and the true cell boundaries and sizes were underestimated by image filtering and segmentation, because only the inside of the cell is captured. Pixels that were brighter than a predetermined threshold were designated bacterial pixels, which were then computationally joined to reconstruct the locations of all bacteria. Then, bacterial geometry information, such as the positions of the centroid and two poles and the length and width of the bacterium, was calculated and collected.

Motility parameters (40), such as instantaneous speed, deviation angle, and MSD, were calculated to characterize the single-cell motility of *M. xanthus* cells. The instantaneous speed was calculated via $|\boldsymbol{r}_{n+1} - \boldsymbol{r}_n|/\Delta t$, where $\boldsymbol{r}_n$ is the cell position vector at frame n and Δt is the time interval between two consecutive frames, and then was smoothed using a 21-point Savitzky-Golay filter. The deviation angle of cell motion was defined as the angle between the cell body axis and the moving direction. MSD of cells was calculated as $\langle \Delta \boldsymbol{r}^2(\tau) \rangle = \langle [\boldsymbol{r}(t + \tau) - \boldsymbol{r}(t)]^2 \rangle$, where $\boldsymbol{r}(t)$ is the position vector of a cell at time t, and τ represents the time interval.

Since the Δ*aglZ* mutant is deficient in moving alone, to improve the statistics, the predation events by the Δ*aglZ* mutant that we analyzed included the events performed both by solitary cells and by individual cells in groups of 2 or 3 cells.

SUPPLEMENTAL MATERIAL

Supplemental material is available online only.

SUPPLEMENTAL FILE 1, PDF file, 1.1 MB.

SUPPLEMENTAL FILE 2, AVI file, 2.1 MB.

SUPPLEMENTAL FILE 3, AVI file, 0.4 MB.

SUPPLEMENTAL FILE 4, AVI file, 0.5 MB.

SUPPLEMENTAL FILE 5, AVI file, 0.5 MB.

SUPPLEMENTAL FILE 6, AVI file, 1.5 MB.

SUPPLEMENTAL FILE 7, AVI file, 0.4 MB.

ACKNOWLEDGMENTS

We thank Tao Chen and Shuang Liu for their help in preparing the RFP-expressing *E. coli*.

This work was supported by the National Key R&D Program of China (2018YFA0902102), the National Natural Science Foundation of China (21621004 and 31570065), and Key Scientific Programs from Shandong Science and Technology Department (2017JHZ009 and 2018GSF121034). The funders had no role in the study design, data collection and interpretation, or the decision to submit the work for publication.

We declare no competing interests.

REFERENCES

1. Bruno JF, Cardinale BJ. 2008. Cascading effects of predator richness. Front Ecol Environ 6:539–546. https://doi.org/10.1890/070136.
2. Pernthaler J. 2005. Predation on prokaryotes in the water column and its ecological implications. Nat Rev Microbiol 3:537–546. https://doi.org/10.1038/nrmicro1180.
3. Seccareccia I, Kost C, Nett M. 2015. Quantitative analysis of *Lysobacter* predation. Appl Environ Microbiol 81:7098–7105. https://doi.org/10.1128/AEM.01781-15.
4. Livingstone PG, Morphew RM, Cookson AR, Whitworth DE. 2018. Genome analysis, metabolic potential and predatory capabilities of *Herpetosiphon llansteffanense* sp. nov. Appl Environ Microbiol 84:e01040-18. https://doi.org/10.1128/AEM.01040-18.
5. Sockett RE. 2009. Predatory lifestyle of *Bdellovibrio bacteriovorus*. Annu Rev Microbiol 63:523–539. https://doi.org/10.1146/annurev.micro.091208.073346.
6. Keane R, Berleman J. 2016. The predatory life cycle of *Myxococcus xanthus*. Microbiology 162:1–11. https://doi.org/10.1099/mic.0.000208.
7. Pérez J, Moraleda-Muñoz A, Marcos-Torres FJ, Muñoz-Dorado J. 2016. Bacterial predation: 75 years and counting! Environ Microbiol 18:766–779. https://doi.org/10.1111/1462-2920.13171.
8. Beebe JM. 1941. Studies on the myxobacteria. 2. The role of myxobacteria as bacterial parasites. PhD dissertation. Iowa State College, Ames, IA.
9. Shimkets LJ. 1999. Intercellular signaling during fruiting-body development of *Myxococcus xanthus*. Annu Rev Microbiol 53:525–549. https://doi.org/10.1146/annurev.micro.53.1.525.
10. Martin MO. 2002. Predatory prokaryotes: an emerging research opportunity. J Mol Microbiol Biotechnol 4:467–477.
11. Muñoz-Dorado J, Marcos-Torres FJ, García-Bravo E, Moraleda-Muñoz A, Pérez J. 2016. Myxobacteria: moving, killing, feeding, and surviving together. Front Microbiol 7:781. https://doi.org/10.3389/fmicb.2016.00781.
12. Rosenberg E, Keller KH, Dworkin M. 1977. Cell density-dependent growth of *Myxococcus xanthus* on casein. J Bacteriol 129:770–777.
13. Berleman JE, Kirby JR. 2009. Deciphering the hunting strategy of a bacterial wolfpack. FEMS Microbiol Rev 33:942–957. https://doi.org/10.1111/j.1574-6976.2009.00185.x.
14. Zhang Y, Ducret A, Shaevitz J, Mignot T. 2012. From individual cell motility to collective behaviors: insights from a prokaryote, *Myxococcus xanthus*. FEMS Microbiol Rev 36:149–164. https://doi.org/10.1111/j.1574-6976.2011.00307.x.
15. Nan B, Zusman DR. 2011. Uncovering the mystery of gliding motility in the myxobacteria. Annu Rev Genet 45:21–39. https://doi.org/10.1146/annurev-genet-110410-132547.
16. Nan B, Zusman DR. 2016. Novel mechanisms power bacterial gliding motility. Mol Microbiol 101:186–193. https://doi.org/10.1111/mmi.13389.
17. Mignot T, Nöllmann M. 2017. New insights into the function of a versatile class of membrane molecular motors from studies of *Myxococcus xanthus* surface (gliding) motility. Microb Cell 4:98–100. https://doi.org/10.15698/mic2017.03.563.
18. Pérez J, Jiménez-Zurdo JI, Martínez-Abarca F, Millán V, Shimkets LJ, Muñoz-Dorado J. 2014. Rhizobial galactoglucan determines the predatory pattern of *Myxococcus xanthus* and protects *Sinorhizobium meliloti* from predation. Environ Microbiol 16:2341–2350. https://doi.org/10.1111/1462-2920.12477.
19. Shi W, Köhler T, Zusman DR. 1993. Chemotaxis plays a role in the social behaviour of *Myxococcus xanthus*. Mol Microbiol 9:601–611. https://doi.org/10.1111/j.1365-2958.1993.tb01720.x.
20. Berleman JE, Scott J, Chumley T, Kirby JR. 2008. Predataxis behavior in *Myxococcus xanthus*. Proc Natl Acad Sci U S A 105:17127. https://doi.org/10.1073/pnas.0804387105.
21. Xiao Y, Wei X, Ebright R, Wall D. 2011. Antibiotic production by myxobacteria plays a role in predation. J Bacteriol 193:4626–4633. https://doi.org/10.1128/JB.05052-11.
22. Gerth K, Jansen R, Reifenstahl G, Hofle G, Irschik H, Kunze B, Reichenbach H, Thierbach G. 1983. The myxalamids, new antibiotics from *Myxococcus xanthus* (*Myxobacterales*). I. Production, physico-chemical and biological properties, and mechanism of action. J Antibiot (Tokyo) 36:1150–1156. https://doi.org/10.7164/antibiotics.36.1150.
23. Daniel K, Gabriela Z, Ole R, Michiel V, Velicer GJ, Rolf M. 2008. Discovering the hidden secondary metabolome of *Myxococcus xanthus*: a study of intraspecific diversity. Appl Environ Microbiol 74:3058. https://doi.org/10.1128/AEM.02863-07.
24. Berleman JE, Allen S, Danielewicz MA, Remis JP, Gorur A, Cunha J, Hadi MZ, Zusman DR, Northen TR, Witkowska HE, Auer M. 2014. The lethal cargo of *Myxococcus xanthus* outer membrane vesicles. Front Microbiol 5:474. https://doi.org/10.3389/fmicb.2014.00474.
25. Wang Y, Li X, Zhang W, Zhou X, Li YZ. 2014. The *groEL2* gene, but not *groEL1*, is required for biosynthesis of the secondary metabolite myxovirescin in *Myxococcus xanthus* DK1622. Microbiology 160:488–495. https://doi.org/10.1099/mic.0.065862-0.
26. Evans AG, Davey HM, Cookson A, Currinn H, Cooke-Fox G, Stanczyk PJ, Whitworth DE. 2012. Predatory activity of *Myxococcus xanthus* outer-membrane vesicles and properties of their hydrolase cargo. Microbiology 158:2742–2752. https://doi.org/10.1099/mic.0.060343-0.
27. Berleman JE, Chumley T, Cheung P, Kirby JR. 2006. Rippling is a predatory behavior in *Myxococcus xanthus*. J Bacteriol 188:5888–5895. https://doi.org/10.1128/JB.00559-06.
28. Berleman JE, Kirby JR. 2007. Multicellular development in *Myxococcus*

xanthus is stimulated by predator-prey interactions. J Bacteriol 189:5675–5682. https://doi.org/10.1128/JB.00544-07.
29. McBride MJ, Zusman DR. 1996. Behavioral analysis of single cells of *Myxococcus xanthus* in response to prey cells of *Escherichia coli*. FEMS Microbiol Lett 137:227–231. https://doi.org/10.1111/j.1574-6968.1996.tb08110.x.
30. Lewenza S, Vidal-Ingigliardi D, Pugsley AP. 2006. Direct visualization of red fluorescent lipoproteins indicates conservation of the membrane sorting rules in the family *Enterobacteriaceae*. J Bacteriol 188:3516–3524. https://doi.org/10.1128/JB.188.10.3516-3524.2006.
31. Rojas ER, Billings G, Odermatt PD, Auer GK, Zhu L, Miguel A, Chang F, Weibel DB, Theriot JA, Huang KC. 2018. The outer membrane is an essential load-bearing element in Gram-negative bacteria. Nature 559:617–621. https://doi.org/10.1038/s41586-018-0344-3.
32. Velkov T, Thompson PE, Nation RL, Li J. 2010. Structure-activity relationships of polymyxin antibiotics. J Med Chem 53:1898–1916. https://doi.org/10.1021/jm900999h.
33. Xiao Y, Gerth K, Müller R, Wall D. 2012. Myxobacterium-produced antibiotic TA (myxovirescin) inhibits type II signal peptidase. Antimicrob Agents Chemother 56:2014–2021. https://doi.org/10.1128/AAC.06148-11.
34. Pan H, He X, Lux R, Jia L, Shi W. 2013. Killing of *Escherichia coli* by *Myxococcus xanthus* in aqueous environments requires exopolysaccharide-dependent physical contact. Microb Ecol 66:630–638. https://doi.org/10.1007/s00248-013-0252-x.
35. Livingstone PG, Millard AD, Swain MT, Whitworth DE. 2018. Transcriptional changes when *Myxococcus xanthus* preys on *Escherichia coli* suggest myxobacterial predators are constitutively toxic but regulate their feeding. Microb Genom 4:e000152. https://doi.org/10.1099/mgen.0.000152.
36. Maier B, Wong GC. 2015. How bacteria use type IV pili machinery on surfaces. Trends Microbiol 23:775–788. https://doi.org/10.1016/j.tim.2015.09.002.
37. Mauriello EM, Zusman DR. 2007. Polarity of motility systems in *Myxococcus xanthus*. Curr Opin Microbiol 10:624–629. https://doi.org/10.1016/j.mib.2007.09.012.
38. Pham VD, Shebelut CW, Diodati ME, Bull CT, Singer M. 2005. Mutations affecting predation ability of the soil bacterium *Myxococcus xanthus*. Microbiology 151:1865–1874. https://doi.org/10.1099/mic.0.27824-0.
39. Zhao K, Tseng BS, Beckerman B, Jin F, Gibiansky ML, Harrison JJ, Luijten E, Parsek MR, Wong GC. 2013. Psl trails guide exploration and microcolony formation in *Pseudomonas aeruginosa* biofilms. Nature 497:388–391. https://doi.org/10.1038/nature12155.
40. Hu W, Gibiansky ML, Wang J, Wang C, Lux R, Li Y, Wong GC, Shi W. 2016. Interplay between type IV pili activity and exopolysaccharides secretion controls motility patterns in single cells of *Myxococcus xanthus*. Sci Rep 6:17790. https://doi.org/10.1038/srep17790.
41. Kaiser D. 1979. Social gliding is correlated with the presence of pili in *Myxococcus xanthus*. Proc Natl Acad Sci U S A 76:5952–5956. https://doi.org/10.1073/pnas.76.11.5952.
42. Wu SS, Kaiser D. 1997. Regulation of expression of the *pilA* gene in *Myxococcus xanthus*. J Bacteriol 179:7748. https://doi.org/10.1128/jb.179.24.7748-7758.1997.
43. Yang R, Bartle S, Otto R, Stassinopoulos A, Rogers M, Plamann L, Hartzell P. 2004. AglZ is a filament-forming coiled-coil protein required for adventurous gliding motility of *Myxococcus xanthus*. J Bacteriol 186:6168–6178. https://doi.org/10.1128/JB.186.18.6168-6178.2004.